applied sciences

MDPI

Article

Finite Element Simulation and Experimental Verification of Circular Tube Nosing through Conical Dies

Walid M. Shewakh [1,2,*] and Ibrahim M. Hassab-Allah [3]

1 Department of Industrial Engineering, Faculty of Engineering, Jazan University, Jazan 82817, Saudi Arabia
2 Mechanical Production Department, Faculty of Technology and Education, Beni-Suef University, Beni-Suef P.O. Box 62521, Egypt
3 Mechanical Design and Production Engineering Department, Faculty of Engineering, Assiut University, Assiut 71516, Egypt; hasa57ibm@yahoo.com
* Correspondence: waleedshewakh@hotmail.com

Abstract: The process of tube nosing is a delicate art that involves forming the end of a tubular part without causing any collapse, buckling, or wrinkling. A recent study has delved into the different modes of failure that can occur during this process and has determined the limits of tube nosing through the use of plasticity and thin/thick-walled tube theories. A finite element simulation was developed to replicate the cold-nosing process using conical dies to validate these theories. The results were compared to experimental outcomes for mild steel, hard steel, and annealed aluminium tubes to ensure accuracy. Through this analysis, we identified and confirmed the modes of failure that can restrict the plastic deformation for the tube nosing process. The outcomes were compared to analytical expressions and showed excellent agreement with the experiments, proving that these expressions provide a reliable reference guide for predicting the limits of the tube-nosing process. The FE simulation method also accurately models critical buckling stresses, nosing loads, and failure modes.

Keywords: forming limits; axial buckling; circumferential buckling; wrinkling; tube-nosing; modes of failure; finite element simulation

check for updates

Citation: Shewakh, W.M.; Hassab-Allah, I.M. Finite Element Simulation and Experimental Verification of Circular Tube Nosing through Conical Dies. *Appl. Sci.* **2024**, *14*, 2337. https://doi.org/10.3390/app14062337

Academic Editor: Alberto Campagnolo

Received: 29 January 2024
Revised: 5 March 2024
Accepted: 7 March 2024
Published: 11 March 2024

1. Introduction

The traditional method for tube nosing involves passing a circular metal tube through conical dies [1,2]. However, it can buckle and fail if the tube wall experiences too much compressive stress during this process. To ensure success, a delicate balance of factors, such as tube geometry, material properties, die geometry, friction at the tube/die interface, and axial feed at the tube ends must be carefully managed. Accurately predicting and controlling buckling is crucial for a successful outcome. A comprehensive understanding of the interaction between the various elements of the tube-nosing process and their boundaries is necessary to create defect-free components. The ultimate goal of tube nosing is to improve part quality while avoiding instability. Maintaining tight control over deformation, rather than simply avoiding excessive die penetration, is one effective method for preventing fracture during tube nosing.

FE simulation is a widely respected technique used in the metal forming industry for designing dies and processes [3,4]. Preventing defects like splitting, buckling, or wrinkling in metal-forming products requires a comprehensive process simulation and verification of metal flow. Process parameters can be examined by conducting FE simulations, and forming loads and failure modes, such as necking, rupture, wrinkling, and excessive springback, can be accurately predicted. Unfortunately, the design of forming tools, material selection, lubricants, and other factors is still based on trial and error, which can be costly. This is highly undesirable in today's competitive environment due to the need for shorter production and turnaround times. Therefore, it is essential to identify the variables present in the metal-forming operation. FE simulation is the most feasible method for identifying the effect of process variables and predicting defects before the actual forming operation takes place [3].

Numerous research studies have analyzed the impact of material properties and process parameters on tube nosing. One of these studies suggested a method to determine the original shell based on the final shape [5], while another created a computer program that uses the same approach to design procedures [6]. Elastic-plastic and rigid-plastic FE simulation techniques have also examined the nosing process [7]. Researchers have used different simulation techniques to analyze the nosing process at room temperature and elevated temperatures [8]. Some have introduced a backward tracing method to determine the optimal preform for shell nosing [9], while others have proposed a preform design method for shell nosing by forward-deformation FE simulation and geometrical modification of the initial shape [10–13]. Different studies have explored the temporary impacts of quasi-static and dynamic internal inversion and nosing in metal tubes [14,15], as well as the non-axisymmetric buckling behavior of circular tubes when subjected to nosing operations using a frictionless conically shaped die [16]. FE simulation has been employed to investigate the cold eccentric tube nosing process of metal tubes utilizing an eccentric conical die [17]. An approximate theory was developed that combines the volume incompressible condition and the Levy–Mises equation to calculate preform shape, nosing ratio, and loading rate in the tube nosing process by spherical die [18]. Lastly, finite element method analysis was used for the tapered die eccentric necking process to investigate the effects of process parameters, such as the initial tube wall thickness, semi-die angle, and friction coefficient [19,20]. The process of double-nosing in tubes was scrutinized. The findings indicated that the experimental and simulation results were congruous. The study disclosed that middle buckling can be curtailed by minimizing the friction coefficient, whereas extending the profile length from 50 to 100 mm can elevate middle buckling while shortening the workpiece length. Furthermore, the research delved into the influence of thermal profiles on the process [21].

Despite previous research on tube nosing, little attention has been paid to the forming limits of the process. This study examines the process limits for cold nosing of metal tubes using analytical expressions and FE simulation with a conical die. The study will investigate the impact of process parameters, such as semi-die angle, coefficient of friction, tube wall thickness, strain hardening exponent, and strength coefficient of tube material, on the limiting nosing ratio and load required for the nosing process.

2. Forming Limits of the Tube-Nosing Process

Tube nosing involves pressing the end of a tube into a spherical or conical die to create a rounded nose. Figure 1 shows an example of tube nosing using a conical die. A tube with specific dimensions is pressed against the die under axial force, causing local bending and contraction near the die inlet. The advancing punch draws the tube inward over the die profile until it eventually inverts, forming a deformed nose. However, if the forming operation is inadequate, axisymmetric or non-axisymmetric buckling may occur, as shown in Figure 2. These defects are unacceptable and depend on tube dimensions, material properties, die geometry, and friction conditions. Failure modes in nosing processes can be grouped into three categories: column buckling, axial buckling, and circumferential buckling of the nosed part.

Euler buckling is a phenomenon that occurs when a tube is nosed and is long and relatively thick. If the tube material has high strength, it can resist the flow through the die cavity, leading to buckling. This usually happens in the initial stages of deformation when the axial compressive stress on the tube wall exceeds the strength of the tube material. Euler buckling happens when the tube collapses due to instability caused by compressive loading. The critical buckling load, F_{cr}, at which the elastic instability of the tube occurs, is defined as the Euler load, and it is given by the following expression:

$$F_{cr} = cEI\left(\frac{\pi}{L}\right)^2 \tag{1}$$

where c is the end condition factor and depends on the tube supporting system, E is the elastic modulus of tube material, I is the area moment of inertia, and L is the tube length.

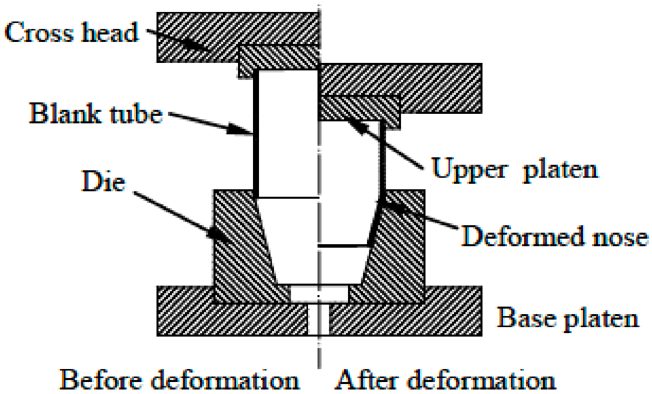

Figure 1. Diagram of the tube-nosing process.

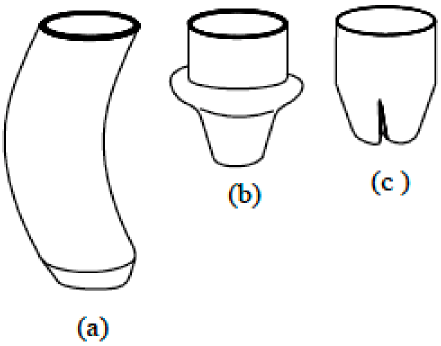

Figure 2. Common failure modes that limit the tube-nosing process; (**a**) column or "Euler buckling", (**b**) axial buckling, (**c**) circumferential buckling.

Euler buckling formulae Equation (1) gives reliable predictions of the global buckling load if the end-conditions are known. The corresponding critical buckling stress σ_{cr1} is calculated as follows:

$$\sigma_{cr1} = \frac{F_{cr}}{A} = cE\left(\frac{\pi r_g}{L}\right)^2 \tag{2}$$

where, A is the cross-sectional area of tube and r_g is the radius of gyration. For a tubular material:

$$r_g^2 = 0.5r^2,\ I = \pi r^3 t,\ A = 2\pi rt$$

where, r is the initial mean radius of tube and t is the initial tube wall thickness.

For the tubular material under buckling conditions, Euler critical buckling stress and Euler critical load can be expressed as follows:

$$\sigma_{cr1} = 0.5cE\left(\frac{\pi r}{L}\right)^2 \tag{3}$$

$$F_{cr} = ctEI\left(\frac{\pi r}{L}\right)^3 \tag{4}$$

In the plastic range, tangent modulus (E_t) of a material is substituted instead of elastic modulus (E) in Equations (3) and (4). The tangent modulus is a function of the material true stress-true strain relation.

Using Hollomon strain hardening expression, the equivalent stress can be expressed as:

$$\overline{\sigma} = K(\overline{\varepsilon})^n \quad (5)$$

where K is the material strength coefficient and n the strain hardening exponent. The slope of the true stress–true strain curve at the critical buckling stress can be obtained as follows:

$$E_t = \frac{d\overline{\sigma}}{d\overline{\varepsilon}} = nK(\overline{\varepsilon})^{n-1} \quad (6)$$

The tube to be nosed must be taken as short as possible to avoid Euler buckling. If altering the design length of the required part is not possible, an inside solid mandrel and/or external supporting sleeve (tube holder) may be used to avoid buckling. For large shell nosing, local annealing prior to the nosing process for the tube part to be nosed may be adopted.

Axial buckling: Under the applied compressive load the tubes may buckle along the axial direction in two ways. This mode of failure normally takes place during the deforming stage when excessive compressive loading is induced through the tube wall. For relatively thin tubes, an axisymmetric bulge-like wave appears on the entire circumference of the tube, near the bottom of the nose. This mode is termed as axisymmetric buckling, as shown in Figure 2. For very thin tubes, irregular waves (axial collapse) appear at the tube end in contact with the machine platen. In either case, the theoretical analysis is similar. For a thin tube, the critical stress σ_{cr2} at which buckling occurs in the elastic range is given by [22]:

$$\sigma_{cr2} = \frac{E_r}{\sqrt{3(1-v^2)}}\frac{t}{r} \quad (7)$$

The critical stress σ_{cr2} causes the tube to undergo instability in form of axisymmetric fold. This formula is applied when buckling occurs at higher stresses. Where (E_r) is the reduced buckling modulus, v is the Poission's ratio. The reduced buckling modulus can be expressed as follows:

$$E_r = \frac{4EE_t}{\left(\sqrt{E}+\sqrt{E_t}\right)^2} \quad (8)$$

Some studies [23] used the tangent modulus (E_t) instead of the reduced buckling modulus E_r for the calculation of critical buckling stress.

Circumferential buckling in tube nosing is a consequence of excessive compressive hoop stress. The part of the tube that is pushed into the die cavity is subjected to compressive hoop stress. As this compressive stress reaches a critical limit, wrinkling will occur. The critical hoop stress depends on the tube geometry and the reduced buckling modulus. The critical compressive hoop stress that initiates buckling on a tube can be calculated using Equation (7). However, in this case, the tangent modulus, which is used to calculate the reduced buckling modulus in Equation (8), represents the slope of the circumferential stress–strain curve at the critical buckling stress.

Limiting nosing ratio (LNR): The nosing ratio (NR) is a quantitative measure used to evaluate the deformation of a tube during the nosing process, which is defined as:

$$NR = 1 - \frac{r_t}{r} \quad (9)$$

where r_t is the throat radius of the nosed part. Every material has a maximum nosing ratio, known as the LNR, that signifies the most significant reduction in the tube throat that can be achieved without experiencing failure. The capacity of a metal tube to nose depends on the tube material's ease of flow in the die cavity and the tube wall material's ability to withstand buckling. The main mechanical properties that affect the tube formability are the strength coefficient K and the strain hardening exponent n. The force applied on the tube during nosing operation, P_n, is given by [2]:

$$P_n = 8\pi K r \left(\frac{2}{\sqrt{3}r_b}\right)^{n+1} \left(\frac{t}{2}\right)^{n+2} \left(\frac{1}{n+2}\right) + 2\pi t r K \left(\frac{2}{\sqrt{3}}\right)^{n+1} \left(\frac{1}{n+1}\right) \left(1 - \frac{r_t}{r}\right)^{n+1} (1 + \mu \cot\alpha) \quad (10)$$

where r_b is the bending radius and α is the semi-die angle. The bending radius r_b can be calculated by the following expression [24]:

$$r_b = tY/[4\sigma_m(1 - \cos\alpha)] \quad (11)$$

where Y is the initial yield stress of the tube material and σ_m is the meridional stress and is approximately equal to the critical buckling stress σ_{cr2}. The critical buckling stress σ_{cr2} may be written in the form,

$$\sigma_{cr2} = P_n/2\pi r t \quad (12)$$

Using Equations (6)–(12) the following expression for the LNR can be obtained

$$LNR = \frac{1}{2}\left\{\left[\frac{2(n+1)}{1+\mu\cot\alpha}\right]\left[\frac{2nEt\left(\sqrt{3}\right)^{n+1}\phi^{n-1}}{r\sqrt{3(1-v^2)}\left[\sqrt{E}+\sqrt{nK\phi^{n-1}}\right]^2} - \frac{1}{n+2}\left(\frac{t}{r_b}\right)^{n+1}\right]\right\}^{\frac{1}{n+1}} \quad (13)$$

where the function ϕ can be determined by the iterative solution of the following equation;

$$\phi = \frac{4nEt}{r\sqrt{3(1-v^2)}\left[\sqrt{E}+\sqrt{nK\varphi^{n-1}}\right]^2} \quad (14)$$

Equation (13) represents the *LNR* as a function of the material properties, tube geometry and friction condition

FE Prediction of Limiting Nosing (LNR)

The forming defects are indicated by the occurrence of an instability point just before complete failure. This point of instability is defined by the peak load that appears at the vicinity of the deformation ends. After this point, the nosed tube is bulged (formation of axisymmetric bulge-like wave) and the nosing load decreases rapidly until complete failure. This is due to the tube wall softening at the bulge zone. The bulge begins with the increase in the tube outer diameter in the radial direction, and the further increase in the nosing load leads to the increase in the tube outer diameter at the bulged zone. Gradually, a larger and larger bulge occurs and the tube finally fails due to axial buckling. In this study, the limiting nosing ratio is calculated when a maximum radial deflection of the bulge reaches 1 mm.

3. Materials and Method

Three metallic tubes, mild steel, hard aluminum, and annealed aluminum, were used in the experiments. Specimens were prepared from tubes with 48 mm outer diameters and 5 mm thicknesses. The specimens were machined on a center lathe. In order to reduce the die–tube interface friction, the outer surface of the tube was carefully fine-machined and polished with a fine grade sand paper (grade 1000). The flow stress of used tubes materials was determined by conducting a uniaxial tension test. The effective stress versus effective strain can be expressed as $\overline{\sigma} = K(\in_o + \overline{\varepsilon})^n$. The material properties are listed in Table 1. The experiments were performed on a 200 kN universal testing machine, utilizing a X-Y recorder to produce a punch load-punch displacement diagram. The rate of loading in the testing machine can be adjusted in the range from 0.1 to 10 divisions per second. All experiments of tube nosing were carried out at a constant speed of 5 mm/min.

Table 1. Material properties characterizing the yield strength.

Material	Stress–Strain Relation σ (MPa)	Yield Stress Y (MPa)	Young's Modulus E (GPa)	Poisson's Ratio v
mild steel, [1]	$\overline{\sigma} = 867(0.00538 + \overline{\varepsilon})^{0.2411}$	332	205	0.33
hard aluminum, [25]	$\overline{\sigma} = 123(\overline{\varepsilon})^{0.194}$	127	70	0.34
ann. aluminum, [25]	$\overline{\sigma} = 134(\overline{\varepsilon})^{0.008}$	72	70	0.34

4. Finite Element Simulations

To analyze the plastic deformation of a circular metallic tube's nosing, we utilize an elasto-plastic FE simulation that assumes isotropic hardening and the von Mises criterion. The problem was accomplished using the ANSYS version 15 package. To make the most of the tube's symmetry, we model only a quarter of the tube and die, as depicted in Figure 3. We assume a perfectly rigid surface for the die due to its high elastic modulus. This is an acceptable approximation since the die's elastic deflection is relatively insignificant compared to the tube's excessive plastic deformation. In the context of tube nosing analysis, the initial mesh of the FE model is shown in Figure 3. The 3-D FE mesh used for the tube consists of 648 solid higher-order elements, each with 20 nodes, including two elements in the thickness direction and 18 in each axial and circumferential direction. The number of elements used for discretization in the finite element mesh varies between 468 and 900, depending on the size of the tube specimen. We simulate the interface between the die and tube through 450 rigid surfaces representing the die's inner surface and flexible surfaces representing the tube's outer surface. The friction at the interface is described using Coulomb's friction law. To model the tube nosing, we move the tube while restricting the movement of the die in all directions. Therefore, all nodes attached to the surface of the tube end, indicated by Arrow C, are coupled to the motion in the Z-direction. We simulate the nosing process by displacing the coupled nodes along the Z-direction.

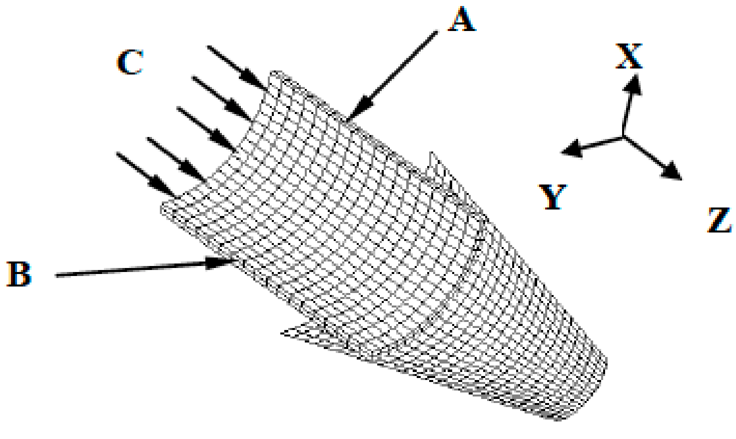

Figure 3. Finite element model showing tube and die for tube nosing.

The nodes connected to the side surface of the tube, as marked by arrows A and B, are constrained in the X- and Y-directions due to their symmetry. Table 2 summarises the forming process parameters utilized in the FE simulation of the tube nosing. The practical and industrial viewpoints were considered when selecting the parameter values. To forecast the possibility of buckling in the tube nosing process, the explicit dynamic FE scheme is used to solve the model. A 3-D four-node shell element is employed to model the tube in this scenario.

Table 2. Properties of the tubes and tooling conditions used for parametric study.

Properties	Values
Strength coefficient, K (MPa)	500, 750, 1000, 1250, 1500
Strain hardening exponent, n	0.1, 0.2, 0.3, 0.4, 0.5
Coefficient of friction, μ	0.05, 0.1, 0.15, 0.2, 0.25
Semi-die angle, ($\alpha°$)	10, 15, 20, 25
Tube outer diameter, D_o (mm)	47
Tube wall length, L (mm) Tube	60, 70, 80, 90, 100
wall thickness, t (mm)	1, 2, 3, 4
Young's modulus, E (Gpa)	205
Poisson's ratio, v	0.33

5. Results and Discussion

Effects of the tube material strength coefficient K on the deformation characteristic of the tube nosing process are analyzed by performing the FE simulation for five different values of K; 500, 750, 1000, 1250, and 1500 MPa. The following process parameters are kept constant; E = 205 GPa, Y = 308 MPa, v = 0.33, n = 0.2, μ = 0.1, D_o = 47 mm, L = 60 mm and t = 2 mm. Figure 4 shows the load–displacement curves during tube nosing for different values of the strength coefficients. It can be noticed that the location of the point of instability (point of the peak load) is not changed by the variation in the strength coefficient. This means that the limiting nosing ratio is not significantly affected by the variation in the strength coefficient of the tube material. Effects of work-hardening behavior for the used tube materials on the nosing load are analyzed by performing the FE simulation for five different values of the n; 0.1, 0.2, 0.3, 0.4, and 0.5. The effects of the strain hardening behavior are carried out for the following constant process parameters: E = 205 GPa, Y = 308 MPa, v = 0.33, K = 1000, μ = 0.1, D_o = 47 mm, L = 60 mm and t = 2 mm. Figure 5 shows the load–displacement curves during tube nosing for different values of the strain hardening exponent. It can be noticed that the die penetration increases with the decrease in the strain hardening exponent. An increase in the die penetration leads to further plastic deformation that can be achieved before the point of instability, i.e., a higher limiting nosing ratio can be reached.

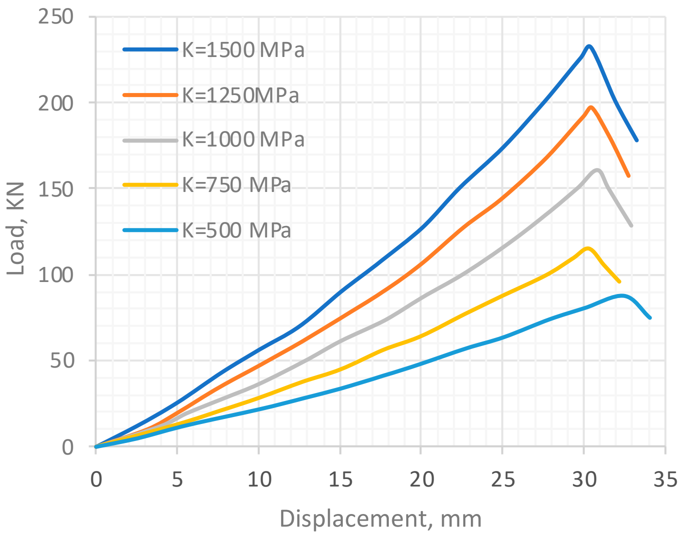

Figure 4. Load–displacement curves for tube nosing with different strength coefficients for E = 205 GPa, Y = 308 MPa, v = 0.33, n = 0.2, μ = 0.1, D_o = 47 mm, L = 60 mm and t = 2 mm.

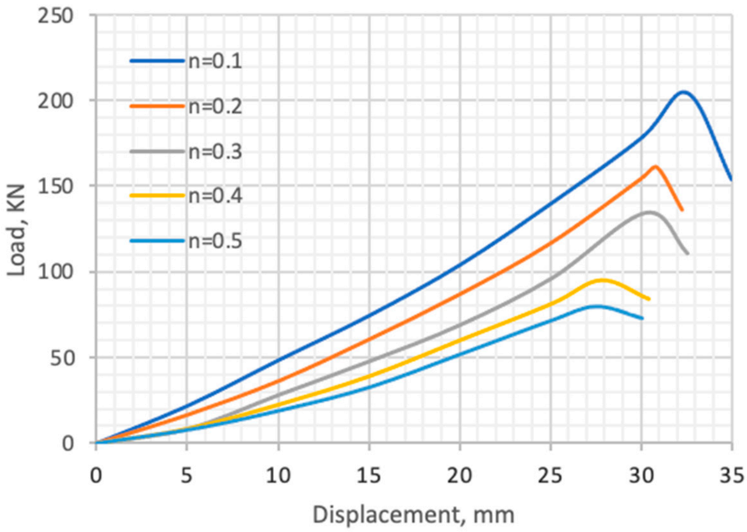

Figure 5. Load–displacement curves for tube nosing with different values of strain hardening exponent for E = 205 GPa, Y = 308 MPa, v = 0.33, K = 1000, μ = 0.1, D_o = 47 mm, L = 60 mm and t = 2 mm.

This result can also be seen in Figure 6, which represents the variations of theoretical, (Equation (13)) and FE values for limiting nosing ratio (LNR) with different values of the strain hardening exponent. This figure indicates that the limiting nosing ratio decreases with the increase in the values of the strain hardening exponent for the tube material. This is because a lower strain-hardening exponent has a lower yield stress in the deformation zone of the tube, which makes the tube nosing easily formed before it fails by buckling. The same tendency is reported in published work [16].

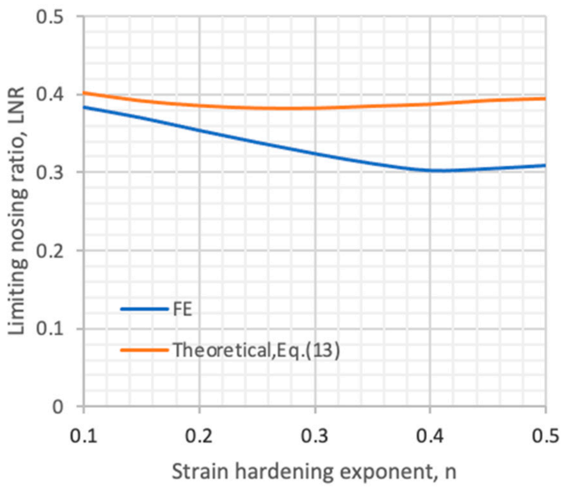

Figure 6. Influence of the strain hardening exponent on limiting nosing ratio for E = 205 GPa, Y = 308 MPa, v = 0.33, K = 1000, μ = 0.1, D_o = 47 mm, L = 60 mm and t = 2 mm.

Effects of friction at the interface of the die and tube are analyzed by performing the FE simulation for five different values of the coefficient of friction, μ = 0.05, 0.1, 0.15 and 0.25 The effects of friction on the deformation characteristic during tube nosing is carried out using the following process parameters E = 205 GPa, Y = 332 MPa, v = 0.33, D_o = 47 mm, L = 60 mm and t = 2 mm. The strain hardening behavior of the tube material is represented by

$$\overline{\sigma} = 867(0.00538 + \overline{\varepsilon})^{0.2411}$$

Figure 7 shows the load–displacement curves during tube nosing for different values of the coefficient of friction μ. The experimental results (from [1]) for the same size of tube specimen are shown accompanied by the FE simulation results (see Figure 7). It can be noticed that the value of the maximum nosing load is not significantly affected by the friction coefficient. Also, the die penetration increases with the decrease in the friction coefficient, i.e., a higher limiting nosing ratio can be achieved. This result can also be seen from Figure 8, which indicates that the limiting nosing ratio decreases with the increase in the friction between the die and the tube. This is because the tube flows into the conical die more easily when there is a lower friction coefficient at the die–tube interface surface.

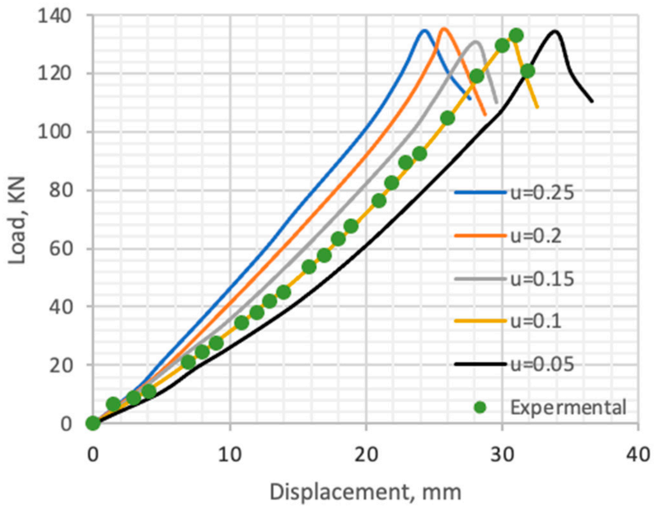

Figure 7. Load–displacement curves for tube nosing with different values of friction coefficients for E = 205 GPa, Y = 332 MPa, v = 0.33, D_o = 47 mm, L = 60 mm, t = 2 mm, and $\overline{\sigma} = 867(0.00538 + \overline{\varepsilon})^{0.2411}$.

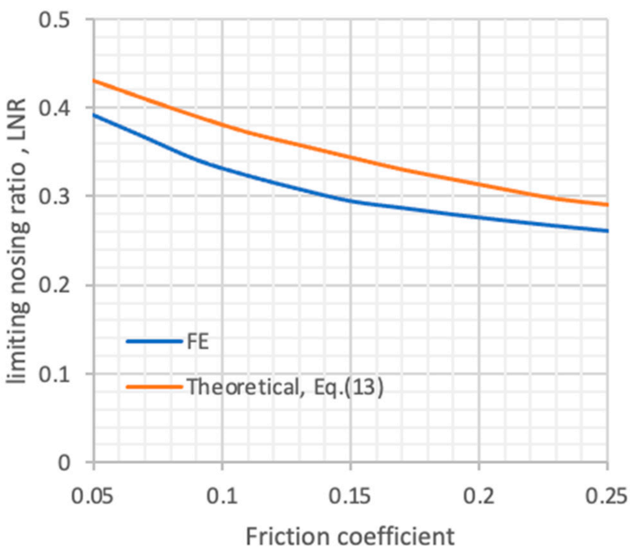

Figure 8. Influence of the friction coefficient on the limiting nosing ratio for E = 205 GPa, Y = 308 MPa, v = 0.33, K = 1000, α = 10°, D_o = 47 mm, L = 60 mm and t = 2 mm.

Effects of the semi-die angle α are analyzed by performing the FE simulation for four different values of α = 10, 15, 20, and 25°. The following parameters are kept constant: E = 205 GPa, Y = 332 MPa, v = 0.33, K = 867, n = 0.241, μ = 0.1, D_o = 47 mm, L = 80 mm and t = 2 mm. Figure 9 shows the load–displacement curves during nosing for different values of the semi-die angle. It can be noticed that, the value of the maximum nosing load is not significantly affected by the variation in the semi-die angle. Also, the die penetration increases with the decrease in the semi-die angle. The quick reduction in the diameter of the formed tube before buckling occurs is a result of a larger die angle. Effects of tube length on the required load for tube nosing are analyzed by performing the FE simulation for five different tube lengths; 60, 70, 80, 90, and 100 mm. The following parameters are kept constant; E = 205 GPa, Y = 332 MPa, υ = 0.33, K = 867, n = 0.241, μ = 0.1, D_o = 47 mm, α = 15° and t = 2 mm. Figure 10 shows the load–displacement curves during nosing for different values of tube length. It can be noticed that both of the die penetrations and the values of the maximum nosing load are slightly affected by the variation in the tube length. The influence of the tube length ranging from 60 mm to 100 mm on the nosing load and LNR is not significant. This result is valid only if the chosen tube length is less than the critical tube length, which leads to Euler buckling.

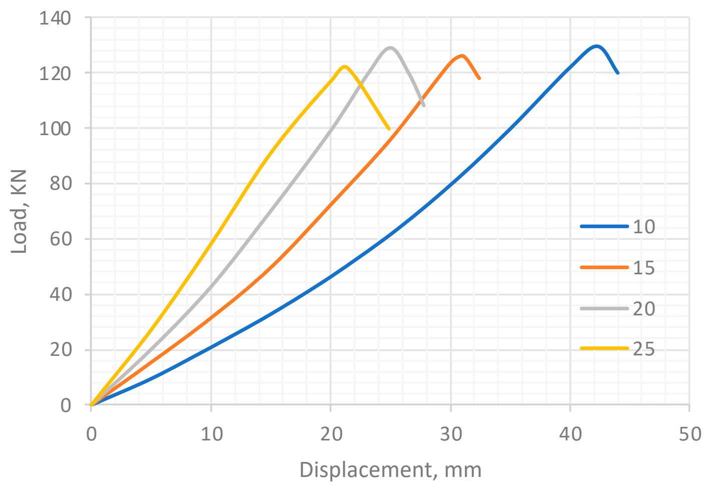

Figure 9. Load–displacement curves for tube nosing with different semi-die angle for E = 205 GPa, Y = 332 MPa, υ = 0.33, K = 867, n = 0.241, μ = 0.1, D_o = 47 mm, L = 80 mm and t = 2 mm.

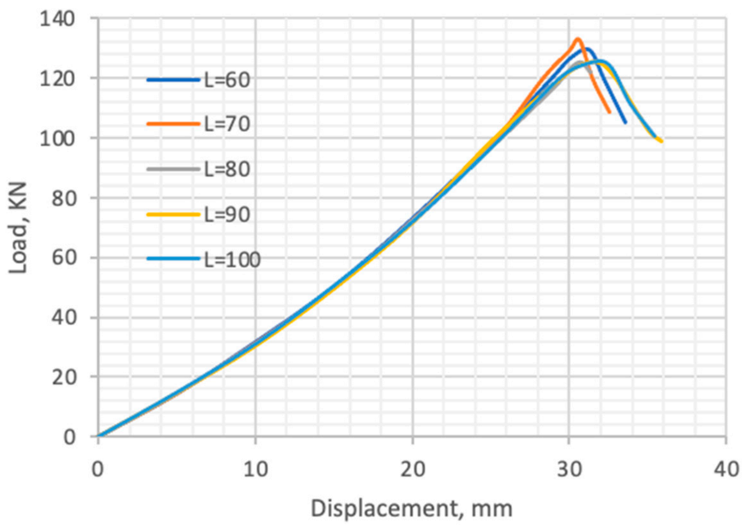

Figure 10. Load–displacement curves for tube nosing with different tube lengths for E = 205 GPa, Y = 332 MPa, υ = 0.33, K = 867, n = 0.241, μ = 0.1, D_o = 47 mm, α = 15° and t = 2 mm.

Effects of tube wall thickness on the required load for tube nosing are analyzed by performing the FE simulation for four different tube wall thicknesses: 1, 2, 3, and 4 mm. The process parameters E = 205 GPa, Y = 332 MPa, υ = 0.33, K = 867, n = 0.241, μ = 0.1, D_o = 47 mm, L = 60 mm and α = 15° are kept constant throughout investigating the effect of the tube wall thickness. Figure 11 shows the load–displacement curves during nosing for different values of tube wall thickness. It can be noticed that both of the die penetrations and the values of maximum nosing load are strongly affected by the variation in the tube wall thickness. The effects of tube wall thickness on the limiting nosing ratio are shown in Figure 12. It can be noticed that the limiting nosing ratio increases with the increase in the tube wall thickness. This is due to the increase in the tube wall stiffness.

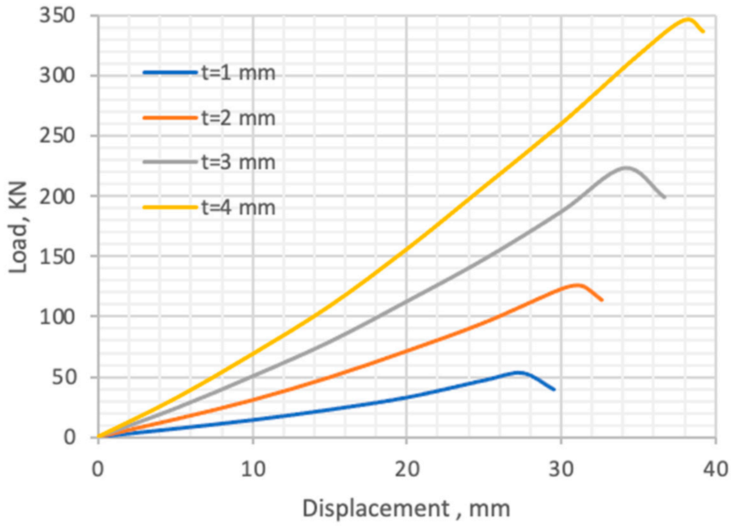

Figure 11. Load–displacement curves for tube nosing with different tube thickness for E = 205 GPa, Y = 332 MPa, v = 0.33, K = 867, n = 0.241, μ = 0.1, D_o = 47 mm, L = *60* mm and α = 15°.

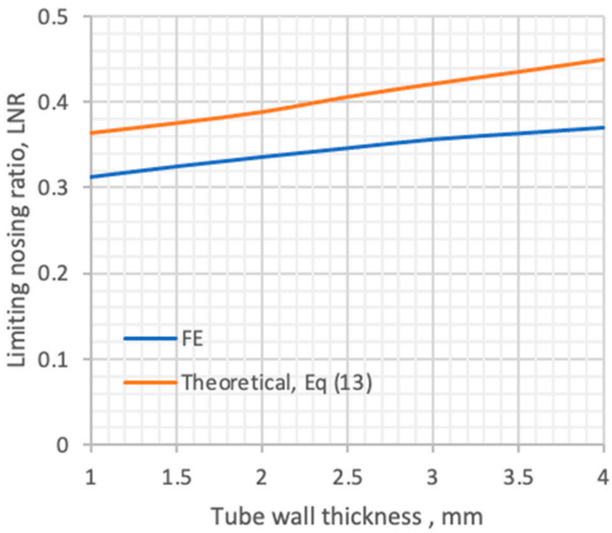

Figure 12. Influence of the tube wall thickness on limiting nosing ratio for E = 205 GPa, Y = 332 MPa, v = 0.33, K = 867, n = 0.241, μ = 0.1, D_o = 47 mm, L = 60 mm and α = 15°.

6. Comparison with Experiments

The accuracy of the proposed FE simulation and analytical expressions in predicting the critical buckling stresses, nosing load, and limiting nosing ratio are verified through comparison with experimental observations. Three different materials, seamless mild steel tube, experimental results from [1], and hard and annealed aluminum tubes A1050 (experimental results from [22]) are used in this analysis. The tube specimen dimensions are as follows: seamless mild steel tubes (outside diameter: 47 mm; tube length: 60 mm, two wall thickness: 2 mm and 0.5 mm), hard and annealed aluminum tubes (outside diameter: 40 mm; wall thickness: 1.5 mm and tube length: 100 mm). The mechanical properties of these tube materials are given in Table 2. Molybdenum disulphide (MoS_2) is used as a lubricant for the aluminum tube specimen and is coated on both the die and the specimen, while PTFE is used as a solid lubricant for the mild steel tube specimen. A thin film of PTFE is wrapped around the outer cylindrical surface of the test specimen.

Comparisons between the experimental, the theoretical and the FE predicted results of critical stresses σ_{cr2} for tube nosed specimen failed by axial buckling mode, see Figure 2b, are given in Table 3. Excellent alignment was achieved between the theoretical, FE, and experimental data. Notably, the critical buckling stress in mild steel tubes surpassed the initial yield stress due to the material's work-hardening under compressive loads. Conversely, the critical buckling stress in hard aluminum tubes was equivalent to the initial yield stress, representing nearly perfect plastic material. Additionally, we compared the experimental nosing load values with the outcomes of the FE simulations. Figure 13 gives comparison of nosing load–displacement curves of the mild steel tube specimen with 2 mm wall thickness and hard aluminum. It is clear from this figure that the FE predicted values match quite well with the experimental results. Experimental values of limiting nosing ratios are compared with that obtained from Equation (13) and FE simulations, as shown in Figure 14. It is clear from this figure that the FE predicted values match quite well with the experimental results. Also, we can observe satisfactory agreements between the theoretical, the finite elements, and the experimental results. Computed modes of failure for mild steel tubes with two different tube wall thickness, 0.5 mm and 2 mm, are also compared, as shown in Figure 15. The comparison of deformed shapes obtained from experimental and FE computational also match well. Usually, only one wrinkle forms on the partially deformed nose. The partially deformed nose has a wrinkle that extends across its entire length and becomes more prominent as the deformation progresses. As the ratio of the tube's outer diameter to its wall thickness decreases, the severity of this wrinkle diminishes. Generally, the occurrence of axisymmetric buckling and wrinkling during the tube nosing are successfully predicted.

Table 3. Comparisons of experimental, theoretical and FE predicted critical stresses σ_{cr2} for tube nosed specimen failed by axial buckling mode.

Material	Experiment σ_{cr2} (MPa)	Theoretical σ_{cr2} Prediction (MPa)	FE Prediction σ_{cr2} (MPa)
mild steel	452	413	440
hard aluminum	130	127	124

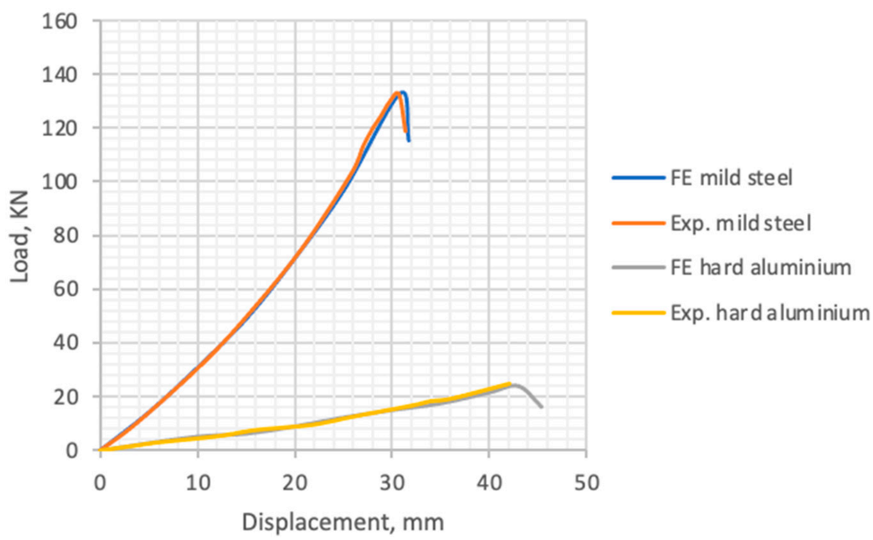

Figure 13. Comparison of the FE predicted and experimental nosing load- displacement (μ = 0.1 and α = 15°).

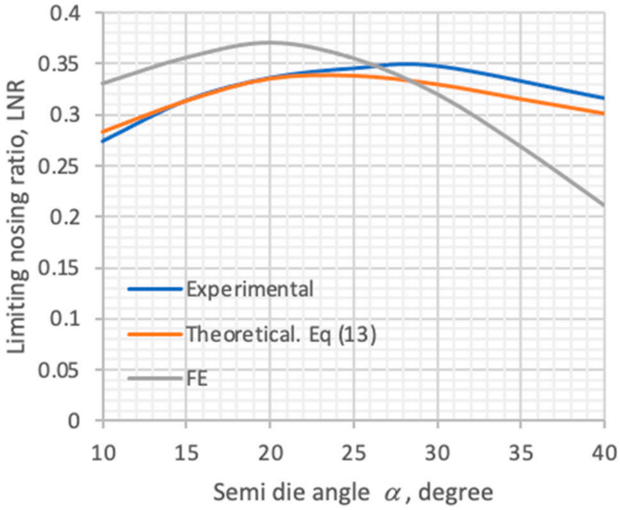

Figure 14. Comparison of the theoretical, FE and experimental LNR for annealed aluminum.

Experimental results for circumferential (*t*=0.5mm)

Experimental results for Buckling axial buckling (*t*=2mm)

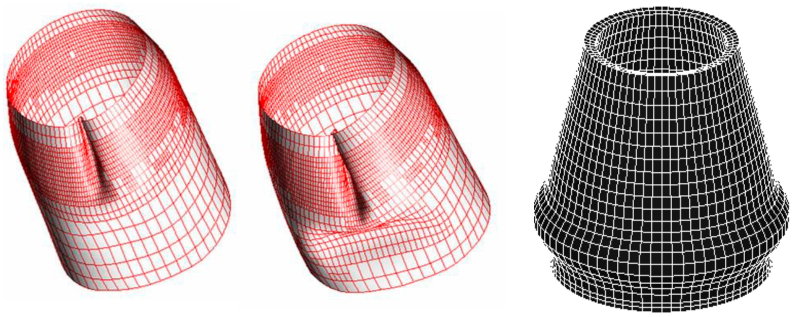

(wrinkling at later stage)

Figure 15. Comparison of the FE predicted and experimental obtained failure modes for E = 205 GPa, Y = 332 MPa, v = 0.33, D_o = 47 mm, L = 60 mm, and $\overline{\sigma} = 867(0.00538 + \overline{\varepsilon})^{0.2411}$.

7. Conclusions

This research delves into the critical buckling stress of tube nosing through analytical and numerical methods to determine its forming limits. The following conclusions can be drawn:

- FE simulation accurately represents the tube nosing process and its failure modes.
- Theoretical predictions, FE predictions, and experimental results of critical buckling stresses align well.
- Simple analytical models can practically compute critical buckling stresses and limiting nosing ratios (LNR), potentially aiding engineers and designers in the early stages of development.

- Tube geometry, including the tube's outer diameter, wall thickness, semi-die angle, friction condition, and material properties, significantly impacts the forming limits of tube nosing.

Author Contributions: Methodology, W.M.S.; Software, W.M.S.; Formal analysis, I.M.H.-A.; Writing—original draft, I.M.H.-A. All authors have read and agreed to the published version of the manuscript.

Funding: This research was funded by the Deputyship for Research and Innovation, the Ministry of Education in Saudi Arabia, project number ISP-2024.

Data Availability Statement: The original contributions presented in the study are included in the article, further inquiries can be directed to the corresponding author.

Conflicts of Interest: The authors declare no conflict of interest.

References

1. Yousef, M.A. Theoretical and Experimental Study on Nose Forming of Metallic Tubes. Master's Thesis, Assiut University, Assiut, Egypt, 2003.
2. Yousef, M.A.; hassab-Allah, I.M.; Ahmed, O.I. Prediction of the forming loads in cold-nosing of metal tubes through conical dies. In Proceedings of the 3rd Assiut University Int. Conf. on Mechanical Engineering Advanced Technology for Industrial Production MEATIP 3, Assiut, Egypt, 24–26 December 2003.
3. Mori, K. (Ed.) *Simulation of Materials Processing: Theory, Methods and Applications*; Toyohashi University of Technology: Toyohashi, Japan, 2001.
4. Wagoner, R.H.; Chenot, J.L. *Metal Forming Analysis*; Cambridge University Press: Cambridge, UK, 2001.
5. Carlson, R.K. An experimental investigation of the nosing of shells. In Proceedings of the Forging of Steel Shells, Annual Meeting of ASME, New York, NY, USA, 29 November–3 December 1943; pp. 45–55.
6. Lahoti, G.D.; Altan, T. Analysis of metal flow in nosing of tubular products. In Proceedings of the 6th North American Manufacturing Research Conference (NAMRC), Manufacturing Engineering Transaction, Gainesville, FL, USA, 16–19 April 1978; pp. 151–157.
7. Huang, Y.; Lu, Y.; Chen, M. Analyzing the cold-nosing process using elasto-plastic and rigid-plastic methods. *J. Mater. Process. Technol.* **1992**, *30*, 351–380. [CrossRef]
8. Tang, M.; Hsu, M.; Kobayashi, S. Analysis of shell nosing-process mechanics and preform design. *Int. J. Mach. Tool Des. Res.* **1982**, *22*, 293–307. [CrossRef]
9. Tang, M.; Kobayashi, S. An investigation of the shell nosing process by the finite-element method. Part 1: Nosing at room temperature (cold nosing). *J. Eng. Ind. Trans. ASME* **1982**, *104*, 305–311. [CrossRef]
10. Park, J.J. Application of the Finite Element Method to Metal Forming Problems. Ph.D. Thesis, University of California, Berkeley, CA, USA, 1982.
11. Park, J.J.; Rebelo, N.; Kobayashi, S. A new approach to preform design in metal forming with finite element method. *Int. J. Mach. Tool Des. Res.* **1984**, *23*, 71–79. [CrossRef]
12. Hwang, S.M.; Kobayashi, S. Preform design in shell nosing at elevated temperatures. *Int. J. Mach. Tools Manuf.* **1987**, *27*, 1–14. [CrossRef]
13. Zhu, J. A new approach to preform design in shell nosing. *J. Mater. Process. Technol.* **1997**, *63*, 640–644. [CrossRef]
14. Ried, S.R.; Harrigan, J.J. Plastic inversion and nosing of metal tubes used as impact energy absorbers. In *Advances in Engineering Plasticity and Applications' 96*; Pergamon Press: Oxford, UK, 1996; pp. 61–66.
15. Ried, S.R.; Harrigan, J.J. Transient effects in the quasi-static and dynamic internal inversion and nosing of metal tubes. *Int. J. Mech. Sci.* **1998**, *40*, 263–280. [CrossRef]
16. Fatnassi, A.; Tomita, Y.; Shindo, A. Non-axisymmetric buckling behavior of elasto-plastic circular tubes subjected to a nosing operation. *Int. J. Mech. Sci.* **1985**, *27*, 643–651. [CrossRef]
17. Kwan, Chin-Tarm An analysis of the eccentric nosing process of metal tubes. *J. Mater. Process. Technol.* **2003**, *140*, 530–534. [CrossRef]
18. Lu, Y.H. Study of preform and loading rate in the tube nosing process by spherical die. *Comput. Methods Appl. Mech. Eng.* **2005**, *194*, 2839–2858. [CrossRef]
19. Nemat-Alla, M. On Eccentric Tube Nosing. *ASME J. Manuf. Sci. Eng.* **2008**, *130*, 011006. [CrossRef]
20. Abdelhameed, R.A.; Alabden, S.; Abdel-rahman, M.; Hassab-Allah, I. Study of aluminum tube cold nosing process into conical and hemispherical dies. *J. Adv. Eng. Trends* **2022**, *41*, 113–124. [CrossRef]
21. Esmailian, M.; Khodadadi, M. Finite Element Simulation of Double-Nosing Process for Manufacturing of the Special Engine Shell. *Arab. J. Sci. Eng.* **2023**, *48*, 11927–11940. [CrossRef]
22. Timoshenko, S.P.; Gere, J.M. *Theory of Elastic Stability*; McGraw-Hill Book, Co.: Haymarket, Australia, 1961.
23. Yang, H.; Sun, Z. Development of a finite element simulation system for the tube axial compressive precision forming process. *In. J. Mach. Tools Manuf.* **2002**, *42*, 15–20.

24. Emara, K.M. *Stress and Strain Analysis in Tube Fluring*; Bulletin of the Faculty of Engineering, Assiut University: Assiut, Egypt, 1990; Volume 18, pp. 26–30.
25. Manabe, K.; Nishimura, H. Nosing of thin-walled tubes by circular curved dies. *J. Mech. Work. Technol.* **1984**, *10*, 287–298. [CrossRef]